remote sensing

Technical Note

Internet-of-Things-Based Geotechnical Monitoring Boosted by Satellite InSAR Data

Denis Guilhot [1,*], Toni Martinez del Hoyo [1], Andrea Bartoli [1], Pooja Ramakrishnan [2], Gijs Leemans [2], Martijn Houtepen [2], Jacqueline Salzer [2], John S. Metzger [2] and Gintaris Maknavicius [3]

1 Worldsensing, 08014 Barcelona, Spain; tmartinez@worldsensing.com (T.M.d.H.); abartoli@worldsensing.com (A.B.)
2 SkyGeo, Inc., San Francisco, CA 94107, USA; pooja.ramakrishnan@skygeo.com (P.R.); G.Leemans@student.tudelft.nl (G.L.); martijn.houtepen@skygeo.com (M.H.); jacqueline.salzer@skygeo.com (J.S.); john.metzger@skygeo.com (J.S.M.)
3 GPS Partneris, 07189 Vilnius, Lithuania; gintaris@gpspartneris.lt
* Correspondence: dguilhot@worldsensing.com

Abstract: Landslides, often a side effect of mining activities, pose a significant risk to humans and infrastructures such as urban areas, power lines, and dams. Operational ground motion monitoring can help detect the spatial pattern of surface changes and their evolution over time. In this technical note, a commercial, cost-effective method combining a network of geotechnical surface sensors with the InSAR data was reported for the first time to accurately monitor surface displacement. The correlation of both data sets is demonstrated in the Gediminas Castle testbed, where slope failure events were detected. Two specific events were analyzed, and possible causes proposed. The combination of techniques allows one to detect the precursors of the events and characterize the consequences of the failures in different areas in proximity to the castle walls, since the solution allows for the confirmation of long-term drifts and sudden movements in real time. The data from the in situ sensors were also used to refine the satellite data analysis. The results demonstrate that not all events pose a direct threat to the safety of the structure monitored.

Keywords: landslide; interferometric synthetic aperture radar (InSAR); geo-information; monitoring; wireless; smart mining; autonomous monitoring; Internet of Things (IoT); connected operational intelligence

Citation: Guilhot, D.; del Hoyo, T.M.; Bartoli, A.; Ramakrishnan, P.; Leemans, G.; Houtepen, M.; Salzer, J.; Metzger, J.S.; Maknavicius, G. IoT-Based Geotechnical Monitoring Boosted by Satellite InSAR Data. *Remote Sens.* **2021**, *13*, 2757. https://doi.org/10.3390/rs13142757

Academic Editor: Nicola Cenni

Received: 13 June 2021
Accepted: 7 July 2021
Published: 14 July 2021

1. Introduction

Land displacements such as mudflows, landslides, topples, or slope failures are triggered by the destabilization of a slope through rainfalls, seismic events, changes in water levels, or human activity, among others. For instance, mining activities such as excavation, blasting, material removal, and water extraction can trigger such events that may compromise worker safety, mine stability, equipment, surrounding communications, and power infrastructure. Landslides result in extensive damages to the environment and infrastructures, and in thousands of lives lost every year, according to the US geological survey [1]. The impact of mining on land stability is significant [2]. Nevertheless, mining is an important component of the global economy. Forty companies share the vast majority of the global mining revenue. In 2019, this represented USD 692 billion [3]. Reducing mining activities is not an option, so reducing their impact of landslides by enabling effective, secure, and qualitative monitoring is essential.

Several methods have been used for slope monitoring and landslide measurements. Terrestrial laser scanning (TLS) and global navigation satellite systems (GNSS) (including global positioning systems (GPS)) are two common techniques used for this purpose [4]. Another one is the synthetic aperture radar interferometry (InSAR) [5,6]. However, land displacements are mostly monitored using a series of sensors disseminated on the ground surface [7]. To detect land motion, or measure its rate, magnitude, and direction, monitoring is conducted using devices such as slope movement sensors (extensometers), accelerometers, inclinometers, tiltmeters, distometers, prisms, survey stations, and vibration sensors [8]. Internet of Things (IoT) monitoring systems are often used for geotechnical information, alone or in combination with innovative technological elements [9–11]. Traditional manual reading is being progressively replaced by the deployment of wireless networks of commercially available instruments to collect, transmit, and process land displacement data, as displayed in Figure 1 for a mining environment. Such monitoring networks have several advantages:

- They do not require human interaction to collect the data;
- They require minimum maintenance;
- They are battery powered;
- They have low power consumption;
- Connectivity to the internet facilitates real-time data visualization and further analyses.

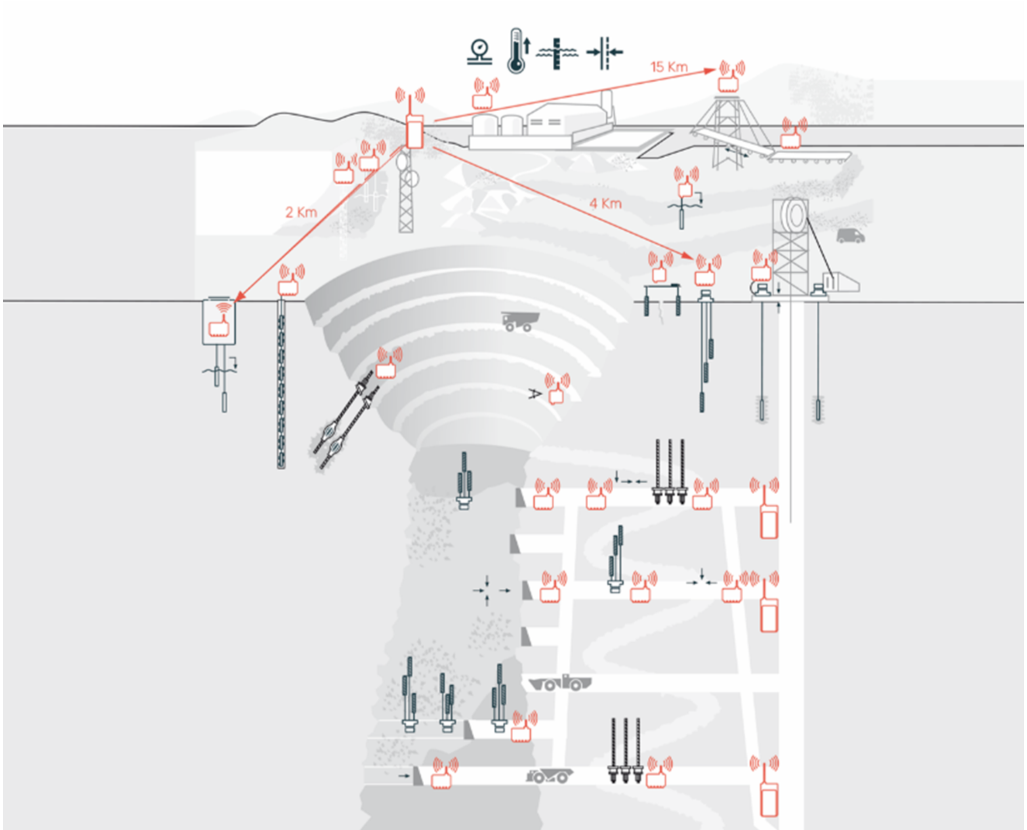

Figure 1. The IoT-based monitoring of a mining site.

Despite these advantages, however, motion sensors provide only discrete information limited to the footprint of the sensor, and a specific time range, resulting in potential information gaps. A considerable amount of work in the field of monitoring has lately been focused on the modeling and forecasting of displacements, to improve monitoring systems while reducing their cost. These predictive systems often exploit the initial geotechnical model of the structure and the data collected by IoT devices is used to update the model and calculate the safety factor of the structure. In particular, PLAXIS 2D and 3D are powerful and user-friendly finite element packages intended for two-dimensional and three-dimensional analyses of displacements and stability in geotechnical engineering and rock mechanics. Nevertheless, it remains generally difficult to detect the long-time precursors of such events. The InSAR technique can be used to identify such precursors, since it allows for analysis over a wide area and a long time period of the trend of slope displacement, velocity, and acceleration, which are the best indicators of ongoing failure processes [12]. Photogrammetry processed aerial photography and the Light Detection and Ranging (LiDAR) survey are also frequently used. Here, we report on a flexible commercial framework, which can orchestrate diverse hardware products and software modules, addressing both large scale and in situ aspects of monitoring.

2. Materials and Methods

2.1. InSAR

Satellite InSAR is commonly used for landslide monitoring and characterization [13], and is also used for slope failure prediction [14]. It has also been used in the mining sector since the first mining displacement map from SAR data was obtained in 1996 [15], although the interest in using spaceborne SAR data to investigate terrain displacement and the integration of instrumentation and monitoring has mainly increased in the past ten years [16]. SAR is a microwave imaging system that enables large-scale coverage independently of the cloud cover and illumination conditions. The SAR signal contains amplitude and phase information. The phase is determined by the distance between the remote sensor and the target on the ground. Differences in phase between multi-temporal scenes of the same target surface enable the mapping of ground displacement and infer surface displacement rates at sub-meter level [17]. Figure 2 depicts the architecture of the proposed solution. A more detailed schematic of the InSAR processing steps was proposed here [18]. As a result of its observational capabilities, SAR has been used to investigate volcanic processes, infrastructure stability and in many more applications, although the most relevant to the work presented here are surface motion, terrain subsidence, landslides and earthquakes [19–22].

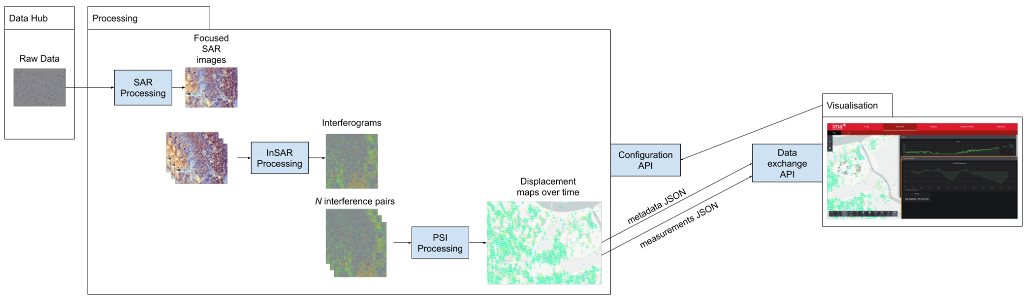

Figure 2. InSAR process simplified schematic diagram.

The InSAR processing was done by SkyGeo with its own proprietary software package for PS (persistent or point-like Scatterer) and DS (distributed scatterer) InSAR data processing [23]. The software and algorithms were developed, improved, and maintained in-house, resulting in complete control of the entire process [24].

The processing chain includes high-precision coregistration to build up a series of aligned SAR images [25]. Either customer-provided or publicly available topographic data were used in the processing to remove the topographic phase component and geocode the interferograms. The data from the in situ sensors were also used to refine the data analysis. For time series analysis, a combined PS and DS processing scheme was applied, after which regional InSAR estimates could be further adjusted using additional independent (e.g., GPS) data. The output product was visualized on a secure web service (SkyGeo Maps).

2.2. Robotic Total Stations (RTS)

An RTS is an automated electro–optical instrument used for monitoring distances and angles from the instrument to a particular point. They can be remotely controlled and used with automated setups. They can also be used in conjunction with a geodetic prism that reflects the laser beam emitted by the RTS. If the reflection is obtained, the polar coordinates of the prism (two angles and the distance) are calculated. Then, the beam is directed to another prism, and the operation repeated for each one of them. If the reflection is not obtained, the total station begins to scan the environment by changing the angles of the laser beam until it detects the prism and reports the new polar coordinates [26]. In this work, Geomax Zoom900 devices were used.

2.3. In Situ Sensors

Engineers have used field observation for a long time and geotechnical asset management has leveraged a widely used, specific methodology known as the observational method, which was first described by Terzaghi [27] and later refined by Peck [28]. It traditionally relies on in situ sensors to provide measurements and instrumentation. The development of affordable geotechnical monitoring devices has enabled the growing relevance of this methodology. Inclinometers such as the ones used in this work have commonly been used since the 1960s. The automation of such monitoring systems was initiated in the 1970s through the smart sensor and remote monitoring paradigm, which have promoted the development of low cost, low power, mostly unattended monitoring systems that can be deployed in vast geographic areas to provide specific monitoring. Together with the emergence of wireless communication technologies, they have enabled the battery-operated, isolated, remote sensing, and monitoring systems used by the geotechnical sector to develop automated solutions [29]. The technology is still evolving towards more innovative IoT-based monitoring systems for improved monitoring and increased safety integrating predictive models, safety factors, cloud components, and artificial intelligence modules [30–32]. The in situ aspect of the technology used in the work reported here is provided by Worldsensing's Loadsensing commercial product, whose architecture is sketched in Figure 3. It is comprised of an IoT data acquisition system and a monitoring solution that combines wireless monitoring and advanced software tools. The main elements of the proposed solution are:

- Sensors (here, inclinometers);
- Distributed low-power nodes;
- Powered gateways;
- Software interface (to configure the devices and manage the wireless network).

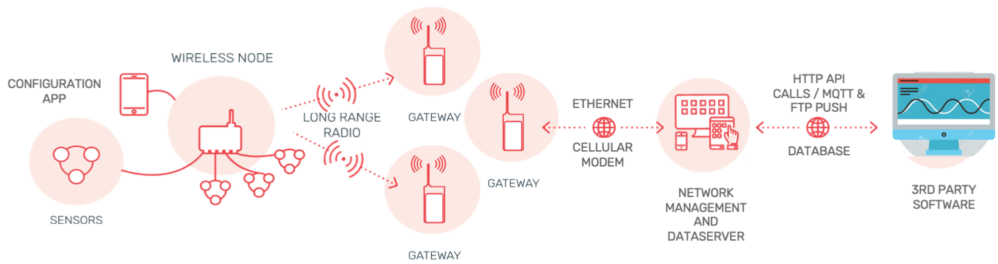

Figure 3. Loadsensing architecture.

The sensors are wired to the dataloggers wireless nodes. These devices send the information of each sensor to the gateway using the long range (LoRa) radio communication protocol. The information is then relayed over ethernet to the network management and dataserver and can be displayed in a visualization software. The real-time data of the sensors and the network is accessible to the user, and is also used to set alarms and warnings.

3. Case Study: Gediminas Castle

3.1. The Problem

Gediminas Castle was built in the 14th century under the command of the Grand Duke of Lithuania Gediminas. It remains a symbol of the Lithuanian state. However, historical sources recorded many landslides over the years on the erosive Gediminas Castle Hill, which represent a risk for the castle conservation. The remaining structures of the castle stand 40 m high, at 138 m above sea level. Geologically, Lithuania is the bottom of the former sea, consisting of sedimentary rocks. The castle hill is composed of quaternary glacial, glaciolacustrine, glaciofliuvial inter-layered deposits and technogenic (cultural layer) accumulations [33]. The years 2016 and 2017 were marked by very heavy rains and all the hillsides were affected by landslides. The first unprecedented slope failures occurred on the northwest slope in February 2017. New landslides were observed in 2020. The consequences of these events are depicted in Figure 4.

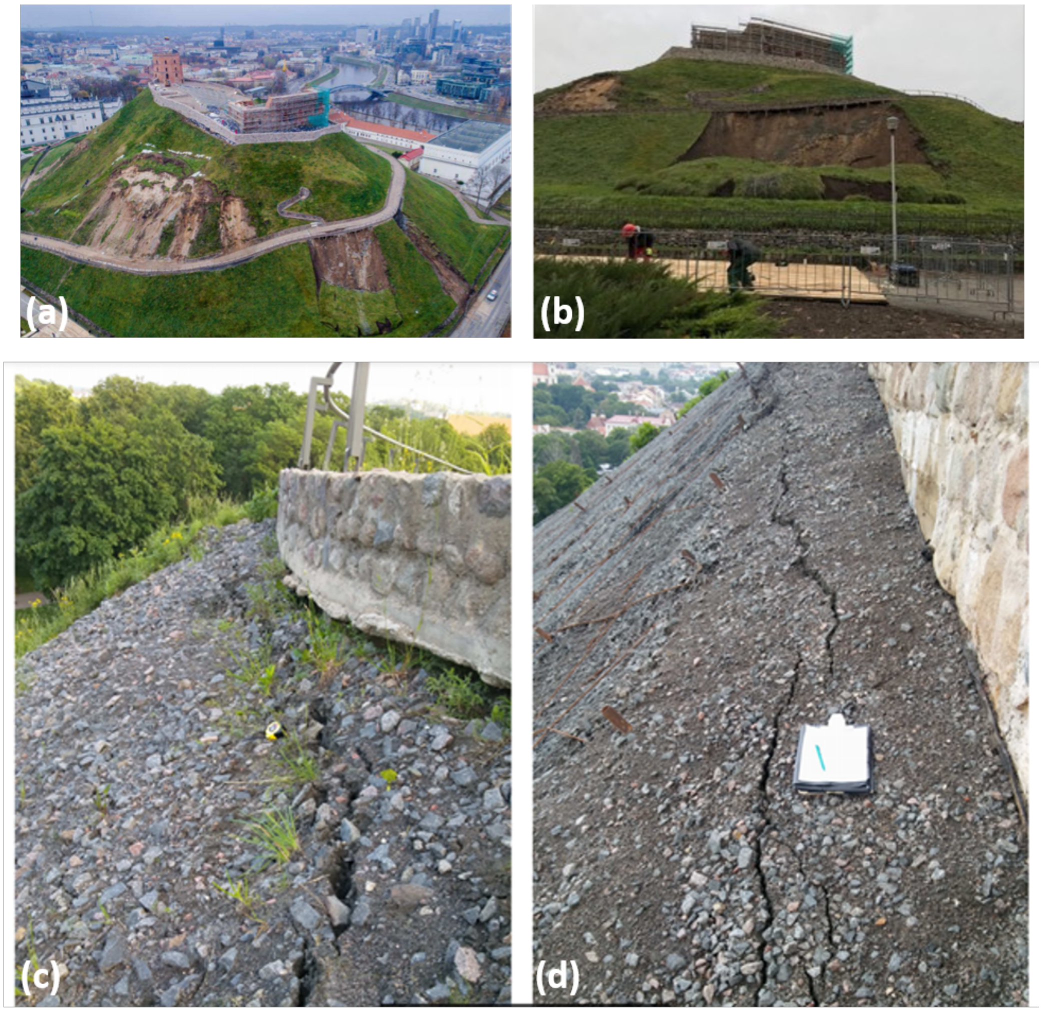

Figure 4. Slope failures on the Gediminas Castle hill: (**a**) November 2017, southeast slope; (**b**) March 2017, northwest slope; (**c**) June 2020, east slope; and (**d**) June 2020, southeast slope. Courtesy of GPS Partneris.

3.2. The Solution

The first recent major slope failure occurred in February 2017 and prompted emergency maintenance works on the hill for slope stabilization, together with installing a digital monitoring system comprising four robotized Geomax Total stations Zoom 900, serving 50 geotechnical prisms in the hill soil, and 28 Loadsensing bi-axial tiltmeters on buildings and defensive and protective ramparts. Measurements are performed every 30 min. The data are sent to a gateway and eventually translated into Vista Data Vision cloud visualization software. The monitoring program also included the installation of total stations and monitoring prisms. During the observation period (2016–2020), the number of sensors was periodically increased, and their location amended, the final location being illustrated in Figure 5. In 2019, the soil reinforcement works were completed; however, the monitoring equipment was left for post-reconstruction monitoring. The InSAR ascending and descending orbits data from Sentinel-1 were analyzed from January 2019 to October 2020 to complete the survey, and the correlation between all three data sets was studied.

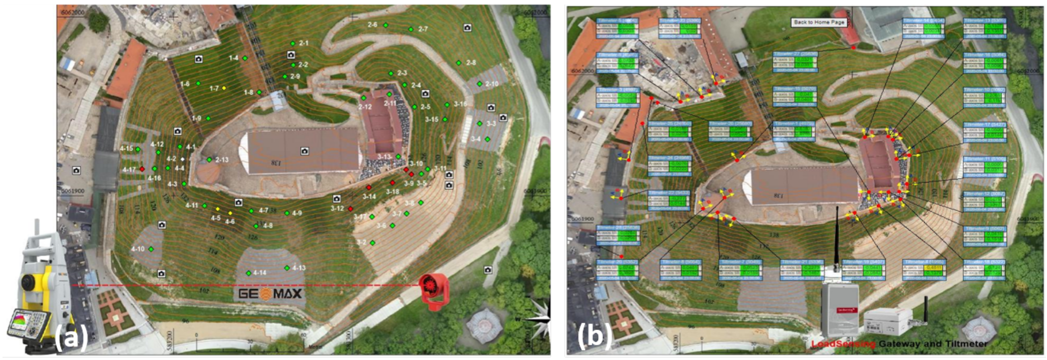

Figure 5. Gediminas Castle instrumentation location: (**a**) total station and prisms; and (**b**) tiltmeters. Courtesy of GPS Partneris.

The tiltmeters are installed on the walls of the castle, at the top and at the bottom of the hill, and some installation examples are displayed in Figure 6.

Figure 6. Gediminas Castle tiltmeters installation examples. Courtesy of GPS Partneris.

3.3. Results

3.3.1. June 2020

A sudden slope failure occurred on the 12th of June 2020.

Robotic Total Stations

The movement was detected by the prisms highlighted in Figure 7.

Figure 8 displays the measurements of the total stations highlighted above.

The approximate magnitude of the movements is detailed in Table 1:

Table 1. Displacement measured by the total stations during the June 2020 event, where plus and minus represent the direction and the number of signs represents the magnitude.

ID	Easting	Northing	Up	Total (mm)
3–10	+ +	+	- -	40
3–12	0	-	-	20
3–14	+	- -	- -	30
3–18	+	-	-	20

Figure 7. Location of the total stations that detected the incident highlighted in yellow.

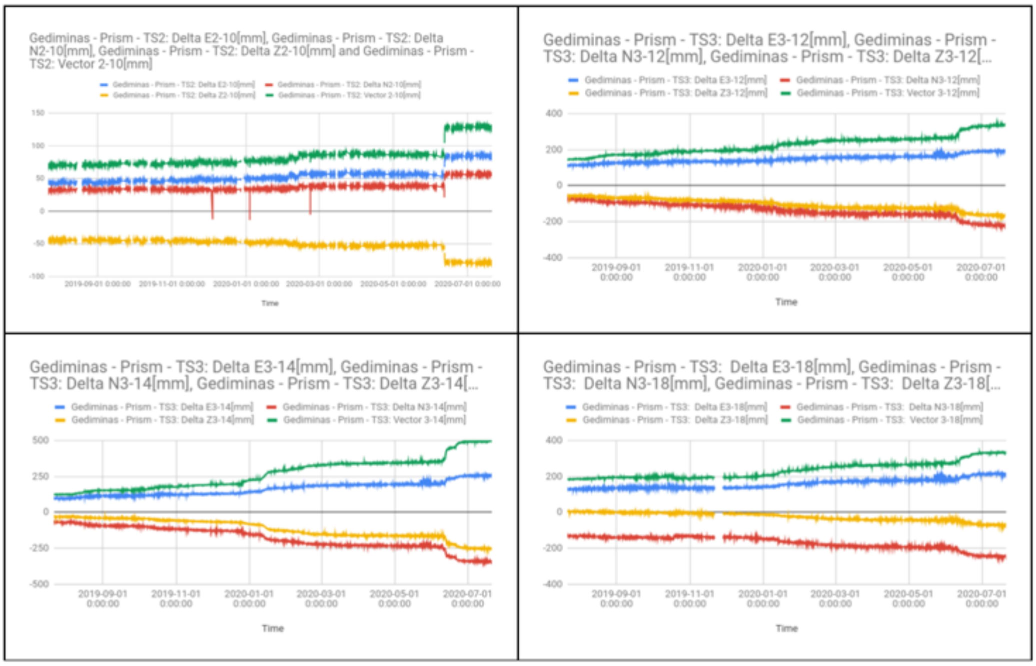

Figure 8. RTS data depicting the movement experienced as a consequence of the June 2020 slope failure.

Tiltmeters

Out of the 11 Loadsensing tiltmeters located on the eastern and southeastern sides of the castle, the four devices whose location is highlighted in yellow in Figure 9 (Top) showed a clear displacement at the moment of the event. The data are plotted in Figure 9 (Bottom).

The displacement is calculated from the angle shift experienced by the tiltmeters, which results in the displacement of the order of the millimeter in both directions. The results are presented in Table 2:

Table 2. Displacement measured by the tiltmeters in the June 2020 event.

Tiltmeter	Displacement in Each Direction (mm)
5062 (T9)	[−1.5;−0.3]
5100 (T11)	[−1.5;1.2]
5322 (T18)	[−0.6;−0.8]
5070 (T15)	[−2;−1.2]

Figure 9. (**Top**) Highlighted tiltmeters detected the event; and (**Bottom**) highlighted tiltmeters data plot.

InSAR

The InSAR results showed that prior displacements clearly preceded the June failure event. The InSAR results exhibit surface displacements across and during the event itself.

In Figure 10, the linear displacement rates of several point scatterers on the slope of the castle hill are presented. SkyGeo's InSAR algorithm has captured several point scatterers that show a large linear rate of displacement (in red) from January to June 2020. The labels indicate the areas of the failures in June (Areas A and B) and July (Area C).

The temporal evolution of the displacement as estimated by InSAR over the time period of the failures is reported below. Figure 11 depicts a point scatterer situated on the southeastern face of the hill, Area A. From the result, it is clear that the slope has been gradually moving since February 2019. Around the time of the first surface event on the 12th of June 2020, the time series indicates a marked increase in the linear rate of displacement (in green). Furthermore, the figure also illustrates that there was an increase in the rate of acceleration of the point in the first few months of 2020 leading up to the actual event. This implies that the slope had begun to move relatively faster prior to the failure event.

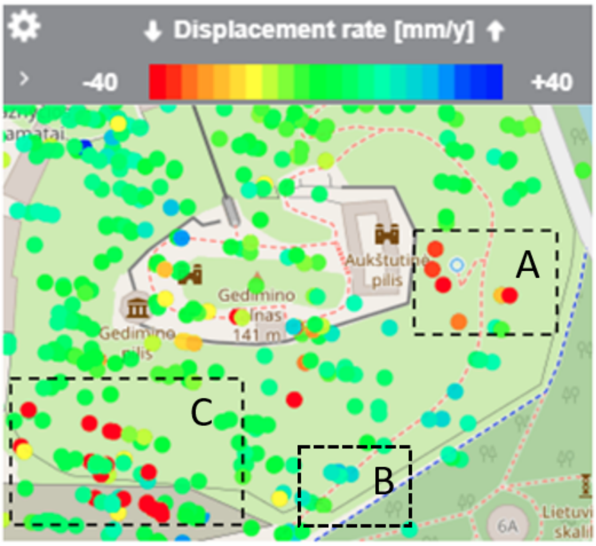

Figure 10. Linear displacement rates before the surface events (January–June 2020).

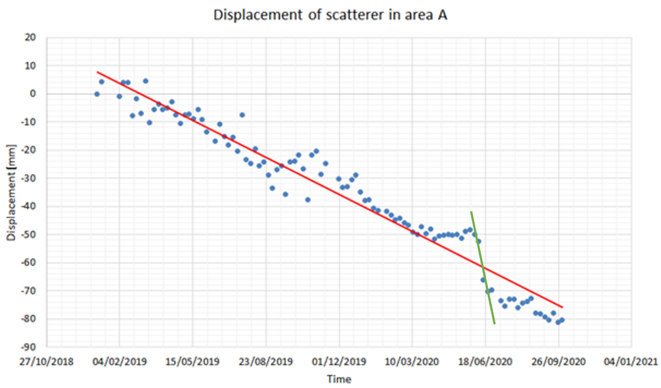

Figure 11. Vertical displacement of scatterer A as a function of time in the area of the June surface event.

A similar result is observed in Figure 12 from another point scatterer situated on the same face of the hill, scatterer B. Here, the gradual displacement from the beginning of 2019 is even more apparent. It also clearly depicts the increased rate of acceleration around December 2019, six months prior to the June 2020 event.

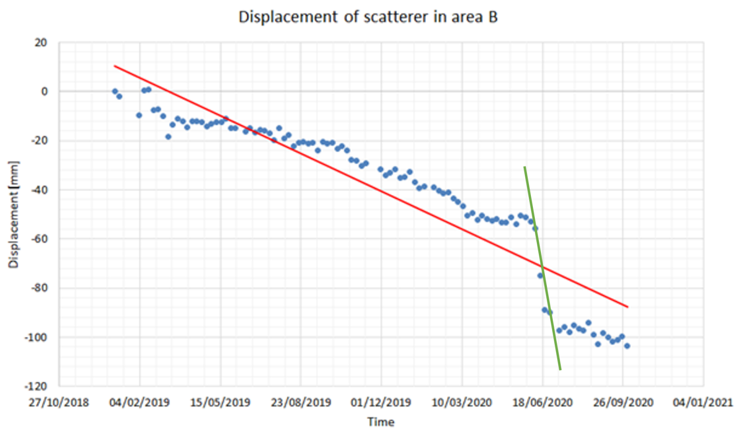

Figure 12. Vertical displacement of scatterer B as a function of time in the area of the June surface event.

3.3.2. July 2020

On the 20th of July 2020, a ground shift was observed on the southwest slope of the Gediminas Castle Hill, the steepest slope of the hill, on the edge of which the tower of the castle stands.

Robotic Total Stations

The movement was detected by the prisms highlighted in Figure 13, whose measurements are displayed in Figure 14.

Figure 13. Total station prisms' locations that detected the July 2020 event.

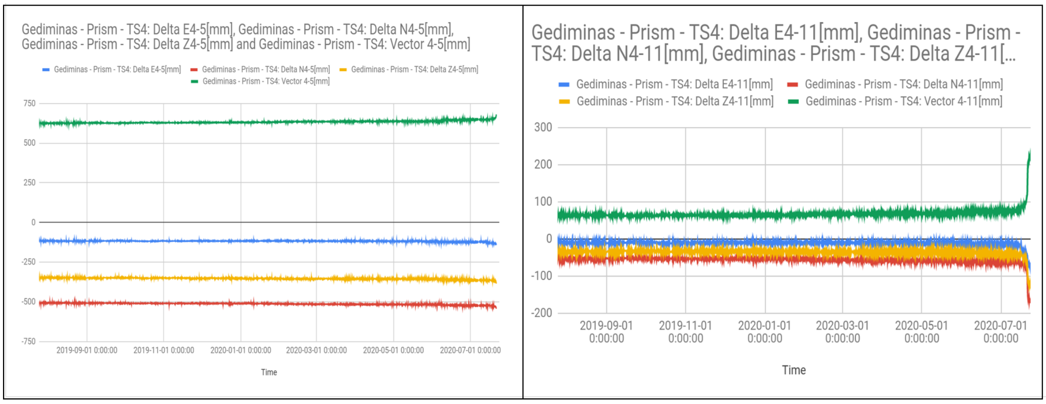

Figure 14. RTS data for the prisms that detected the July 2020 event.

The approximate magnitude of the movements is detailed in Table 3:

Table 3. Vertical displacement measured by the total stations during the July 2020 event.

ID	Easting	Northing	Up	Total (mm)
4–5	-	-	-	30
4–11	- -	- -	- -	150

Here, minus represents the direction and their number represents magnitude.

Tiltmeters

Figure 15 presents the results of the Loadsensing tiltmeters located in the region of interest of the event. No significant displacements were observed during July 2020 by any of the tiltmeters.

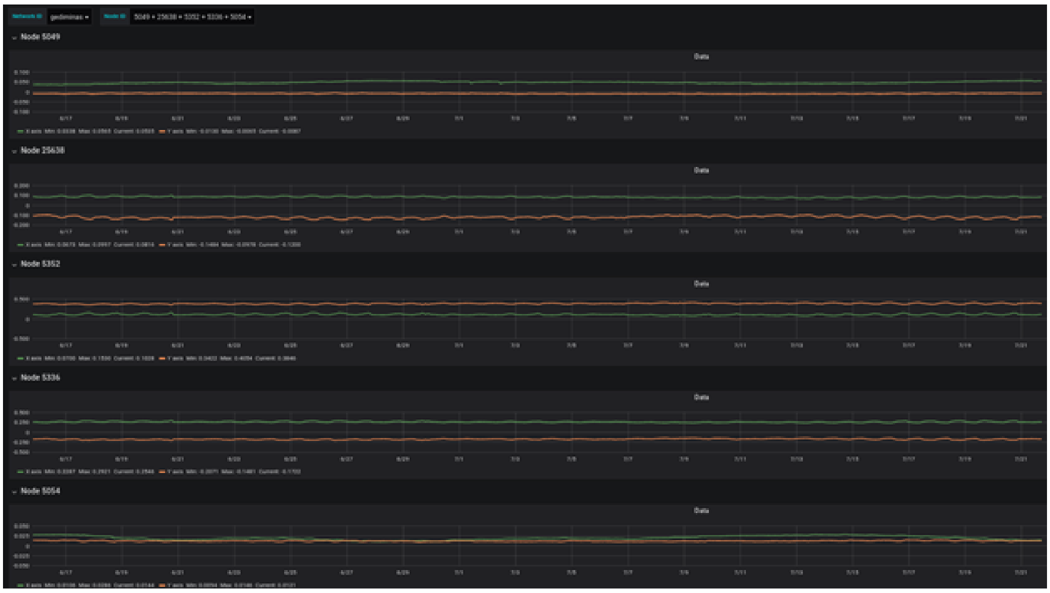

Figure 15. Tiltmeters data in the region of interest during the July 2020 event.

InSAR

The failure in July is noted in the InSAR data, however, it showed limited displacements preceding the event. The displacement rates in Area C are lower than in area A and B (June 2020) when considering the entire time period. However, when considering only a shorter time period preceding the failures (January–July 2020), we found that in area C, some scatterers showed higher displacement rates (see Figure 10).

Figure 16 depicts a point scatterer situated on the southwestern face of the hill, Area C. Compared to the eastern and southeastern faces, this facade remained relatively stable up until early 2020. There is increased acceleration from March 2020 with a sharp increase in subsidence around June 2020. The point scatterer rapidly moved until the slope failure occurred on this front on the 20th of July 2020 after which the signal decelerated but continued to remain unstable.

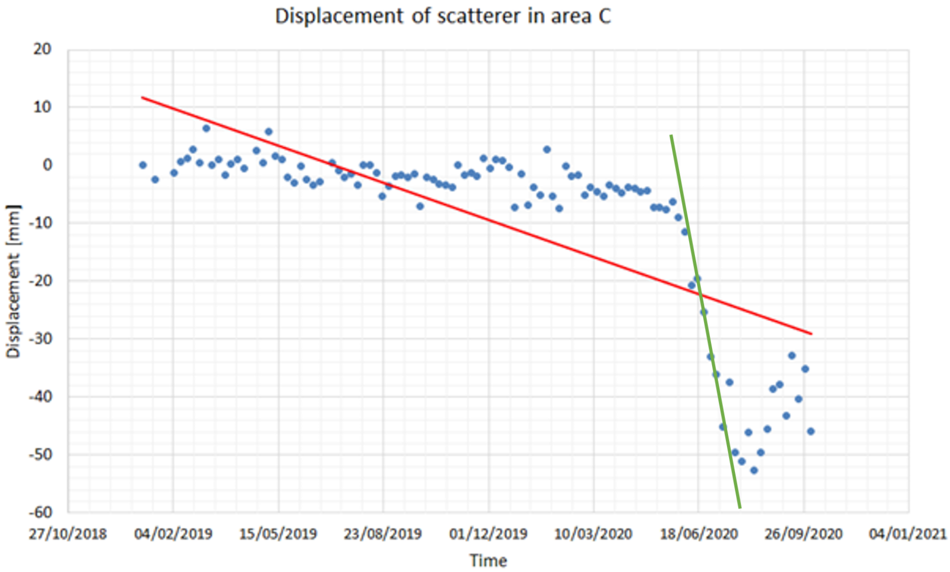

Figure 16. Displacement of scatterer in Area C as a function of time in the area of the July surface event.

4. Discussion

The data collected from each of the sources were compared with the visual inspection of both the events observed in June and July 2020. A strong correlation was reported between the actual events and the robotic total stations information since the prisms were installed on the hill slopes themselves. False positives and false negatives were not observed, while the direction of the vector of the displacements matches the expected direction, given the contour lines.

2020 was the warmest year on record in Lithuania. The average annual temperature measured was of 9.2 °C. This was 2.3° above the multi-annual average. The year 2020 was also relatively dry in Lithuania since the total amount of precipitation was 7% less than a normal year [34]. June and July are typically two months with heavy rainfall in Vilnius, which are condensed in few days. In particular, in 2020, there were several days of heavy rain in the beginning of June, just before the slope failure event observed. During July, the weather was mainly dry, although heavy rains were reported on the same day of the slope failure event. These rains could have triggered the specific events, although the general trend displayed in Figures 11 and 12 demonstrates that such events are to be expected.

Since the tiltmeters are located on the castle walls, they measure the effects of the incidents on the structure, rather than the incidents themselves. The Loadsensing data show minor changes during the June 2020 event in the tiltmeters located in the same direction away from the castle, while tiltmeters outside the region of interest (ROI) do not detect the event, as reported in Table 4. The measurements were also reported in Figure 17 and are consistent with the expected behavior.

Table 4. Summary of the displacements measured during the June 2020 event.

RTS ID	RTS Disp. (mm)	Tiltmeter ID	Tiltmeter Disp. Axis 1 (mm)	Tiltmeter Disp. Axis 2 (mm)	InSAR Scatterer ID	InSAR Short Term Disp. (mm)	InSAR Long Term Disp. (mm)
3–10	40	5062 (T9)	−1.5	−0.3	A	−13	−80
3–12	20	5100 (T11)	−1.5	1.2	B	−18	−100
3–14	30	5322 (T18)	−0.6	−0.8	-	-	-
3–18	20	5070 (T15)	−2	−1.2	-	-	-

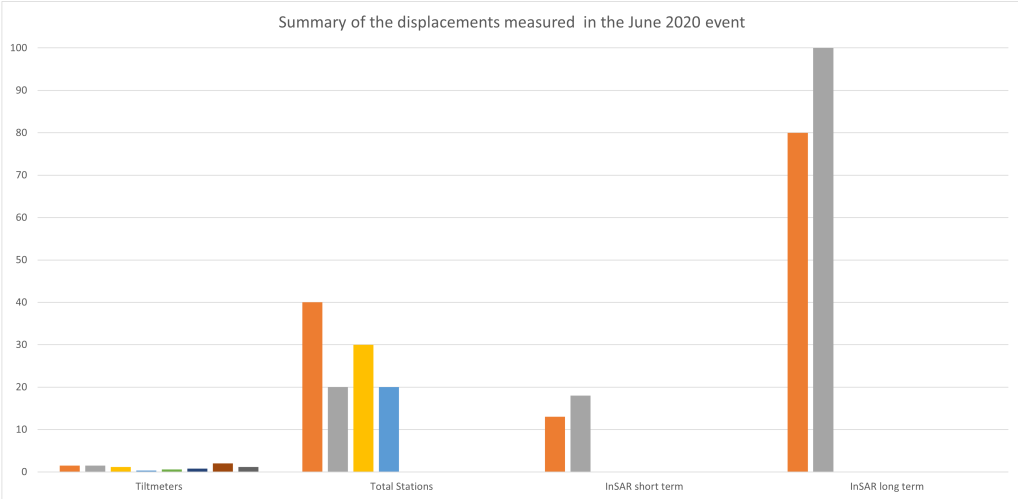

Figure 17. Summary graph of the displacements measured in the June 2020 event.

The magnitude of the event, as reported by the tiltmeters in the ROI, has a smaller scale than the one from the total stations. This is also consistent with expected results since the tiltmeters are installed on a more stable structure (the castle itself, located at the top of the hill, and the castle walls located at the bottom of the hill) whilst the landslide event occurred on the slopes. The tiltmeters did not detect a trend in the movement but a sudden change, which is also consistent with the type of slope failure observed: a sudden landslide. This makes it difficult to detect trends or patterns that can be observed in other scenarios.

The tiltmeters did not detect the July event, as reported in Table 5, even in the ROI, which demonstrates that, although the hill slopes have experienced a slope failure event, the castle itself was not affected. This illustrates the fact that the displacement of the surrounding area does not always pose a threat to the structure and infrastructure being monitored. Nevertheless, the long-term shift detected by InSAR is also a precursor of future slope failure events.

Table 5. Summary of the displacements measured in the July 2020 event.

RTS ID	RTS Disp. (mm)	Tiltmeter ID	Tiltmeter Disp. Axis 1 (mm)	Tiltmeter Disp. Axis 2 (mm))	InSAR Scatterer ID	InSAR Short Term Disp. (mm))	InSAR Long Term Disp. (mm))
4–5	30	5336	-	-	C	−5	−53
4–11	150	5049	-	-	-	-	-
-	-	5352	-	-	-	-	-
-	-	5054	-	-	-	-	-
-	-	25,638	-	-	-	-	-

The results described in Section 3.3 point towards the wide applicability of InSAR for the estimation of displacements in cases of slope instability and failure. The success of the approach appears to vary between failure events and specific scatterers. In this observation of medium resolution Sentinel-1 data, the coverage of the slopes by the InSAR measurements is not totally spatially consistent. This may be explained by one of the key assumptions of robust InSAR data being consistent and persistent reflection results over time. Furthermore, sudden displacements may lead to errors in the displacement estimation. As indicated by Figure 16, the slope failure on the southwestern front was a large and sudden movement with a magnitude of displacement that is relatively difficult for this InSAR analysis (temporal and spatial resolution constraints) to capture. At the castle hill area of interest, the incidence angle and geometry of the slope compounded the challenges in correlating coherent signals with the event.

In comparison, the combination of InSAR with other technologies has been extensively validated, for instance with LiDAR [35], GNSS [36,37], and other remote sensing techniques such as ground-based radar [38]. InSAR has also been used to study slope failure events in open pit mines and show how the technique could be used to detect precursor signs of catastrophic slope failure [36]. The combination of InSAR with 2D finite element models [39] and 3D slope stability software [40] has also been reported. Nevertheless, there are still few studies of the combination of InSAR with underground and terrestrial structural monitoring. Selvakumaran et al. have reported comparable InSAR and automated total station (ATS) readings [41]. In this specific work, the comparison of InSAR and ATS readings turned out to be comparable regarding the relative movement of points along the bridge from one another, although there was no data correlation of InSAR with other types of in situ sensors. Lastra et al. reported a high correlation between GNSS and InSAR measurements without correlation with the extensometer measurements [42]. The Earth Dam of Conza della Campania was monitored with a combination of extensometers and InSAR, showing a strong agreement between the displacements recorded by both monitoring techniques [43]. Finally, the comparison of InSAR results with in situ monitoring by inclinometers was reported, which validates InSAR as a valuable technique to monitor landslide displacements [44,45].

The results proposed here demonstrate the complementarity of both techniques. This might be relevant for applications in mining monitoring, where slope failures frequently occur, especially for open pit mines, quarries, and Tailings dams. Future work will include the validation of the technology in real dormant and active mining sites, as well as the inclusion of other types of sensors relevant for mining monitoring, such as in-place inclinometers. Further steps for this work will also address the improvement of the metadata for the RTS and Loadsensing, mainly regarding location and orientation, and will be solved by working on different use cases. Agreements have been reached for new testbeds in an active open pit mine and a tailing storage facility. These new testbeds will also allow the validation of this method in real mining scenarios. Other steps might involve the development of numerical simulations of landslide failures to interpret the measured result [46,47], and the application of relevant aspects of the theory of mining area displacement.

5. Conclusions

The authors report here the successful implementation and validation of a commercial monitoring system which correlates the data from IoT data acquisition and monitoring system with other data sources (robotic total stations and the SkyGeo InSAR) in a real testbed. The data are correlated in one slope failure event, where all three technologies have detected displacements in the same directions, with different orders of magnitude consistent with the location of the sensors. In another event, the RTS and InSAR detected the event in a correlated manner whilst the tiltmeters demonstrated that the structure was not affected.

Furthermore, the complementarity of both technologies is demonstrated, since the InSAR data observe ground displacement on a large scale and over a large period of time, detecting displacement precursors before the slope failure events occurred, whilst the IoT system detects the actual consequences on the structure being monitored. The in situ sensors data are also used to optimize the InSAR data analysis.

Author Contributions: Conceptualization, D.G.; methodology, D.G.; software, T.M.d.H., P.R. and G.L.; validation, D.G., T.M.d.H. and G.M.; formal analysis, T.M.d.H.; investigation, D.G., T.M.d.H., P.R. and G.M.; resources, P.R. and T.M.d.H.; data curation, D.G., T.M.d.H., P.R. and G.L.; writing—original draft preparation, D.G., J.S. and P.R.; writing—review and editing, T.M.d.H., A.B., J.S.M., M.H., J.S. and G.L.; visualization, T.M.d.H.; supervision, D.G., M.H. and J.S.M.; project administration, D.G.; funding acquisition, D.G. and A.B. All authors have read and agreed to the published version of the manuscript.

Funding: This activity has received funding from European Institute of Innovation and Technology (EIT), a body of the European Union, under the H2020, the EU Framework Programme for

Research and Innovation. This publication is funded by the EIT RAW MATERIAL project AMICOS: Autonomous Monitoring and Control System for Mining Plants—Project Number 19018.

Institutional Review Board Statement: Not applicable.

Informed Consent Statement: Not applicable.

Data Availability Statement: The data presented in this study are available on request from the corresponding author. The data are not publicly available due to privacy reasons.

Acknowledgments: The authors wish to acknowledge the help of GPS Partneris, who allowed access to the data. The authors are also grateful to Angela Lluch and Juan Perez at Worldsensing, who helped with the data interpretation.

Conflicts of Interest: The authors declare no conflict of interest.

Abbreviations

The following abbreviations are used in this manuscript:

2D	2-Dimensional
3D	3-Dimensional
ATS	Automated Total Station
DS	Distributed Scatterer
GNSS	Global Navigation Satellite System
GPS	Global Positioning System
IoT	Internet of Things
InSAR	Synthetic Aperture Radar Interferometry
LoRa	Long Range
LOS	Line of Sight
PS-InSAR	Persistent Scatterer Synthetic Aperture Radar Interferometry
ROI	Region of Interest
RTS	Robotic Total Station
SAR	Synthetic Aperture Radar
TLS	Terrestrial Laser Scanning

References

1. US Geological Survey. Available online: https://www.usgs.gov/natural-hazards/landslide-hazards (accessed on 9 April 2021).
2. Senouci, O. Mining: A Key Human Cause of Landslides. *Int. Res. J. Eng. Technol.* **2020**, *7*, 6604–6606.
3. Mining—Statistics and Facts. Available online: https://www.statista.com/topics/1143/mining/#:~:text=Consequently (accessed on 7 April 2021)
4. Barbarella, M.; Fiani, M. Monitoring of large landslides by Terrestrial Laser Scanning techniques: Field data collection and processing. *Eur. J. Remote Sens.* **2013** *46* 126–151. [CrossRef]
5. Singhroy, V.; Mattar, K.E.; Gray, A.L. Landslide characterisation in Canada using interferometric SAR and combined SAR and TM images. *Adv. Space Res*. **1998**, *21*, 465–476. [CrossRef]
6. Massonnet, D.; Feigl, K.L. Radar interferometry and its application to changes in the Earth's surface. *Rev. Geophys*. **1998**, *36*, 441–500. [CrossRef]
7. Zaki, A.; Chai, H.K.; Razak, H.A.; Shiotani, T. Monitoring and evaluating the stability of soil slopes: A review on various available methods and feasibility of acoustic emission technique. *Comptes Rendus Geosci.* **2014**, *346*, 223–232. [CrossRef]
8. Highland, L.M.; Bobrowsky, P. Appendix B. Introduction to Landslide Evaluation Tools—Mapping, Remote Sensing, and Monitoring of Landslides. In *The Landslide Handbook—A Guide to Understanding Landslides*; U.S. Geological Survey Circular: Reston, VI, USA, 2008; pp. 65–74.
9. El Moulat, M.; Debauche, O.; Mahmoudi, S.; Brahim, L.A.; Manneback, P.; Lebeau, F. Monitoring System Using Internet of Things For Potential Landslides. *Procedia Comput. Sci.* **2018**, *134*, 26–34. [CrossRef]
10. Abraham, M.T.; Satyam, N.; Pradhan, B.; Alamri, A.M. IoT.based Geotechnical Monitoring of Unstable Slopes for Landslide Early Warning in the Darjeeling Himalayas. *Sensors* **2020**, *20*, 2611. [CrossRef] [PubMed]
11. Elavarasi, K.; Nandhini, S. Landslide Monitoring and Tracking Using IoT Sensors. *J. Phys. Conf. Ser.* **2021**, *1717*, 012060. [CrossRef]
12. Carlà, T.; Intrieri, E.; Raspini, F.; Bardi, F.; Farina, P.; Ferretti, A.; Colombo, D.; Novali, F.; Casagli, N. Perspectives on the prediction of catastrophic slope failures from satellite InSAR. *Nat. Res. Sci. Rep.* **2019**, *9*, 14137. [CrossRef] [PubMed]
13. Aslan, G.; Fournelis, M.; Raucoules, D.; De Michele, M.; Bernardie, S.; Cakir, Z. Landslide Mapping and Monitoring Using Persistent Scatter Interferometry (PSI) Technique in the French Alps. *Remote Sens.* **2020**, *12*, 1305. [CrossRef]

14. Wasowski, J.; Bovenga, F. Investigating landslides and unstable slopes with satellite Multi Temporal Interferometry: Current issues and future perspectives. *Eng. Geol.* **2014**, *174*, 103–138. [CrossRef]
15. Carnec, C.; Massonnet, D.; King, C. Two examples of the use of SAR interferometry on displacement fields of small spatial extent. *Geophys. Res. Lett.* **1996**, *23*, 3579–3582. [CrossRef]
16. Colombo, D.; MacDonald, B. Using advanced InSAR techniques as a remote tool for mine site monitoring. In Proceedings of the International Symposium on Slope Stability in Open Pit Mining and Civil Engineering, Nantes, France, 12–14 October 2015.
17. Ma, C.; Cheng, X.; Yang, Y.; Zhang, X.; Guo, Z.; Zou, Y. Investigation on Mining Subsidence Based on Multi-Temporal InSAR and Time-Series Analysis of the Small Baseline Subset—Case Study of Working Faces 22201-1/2 in Bu'ertai Mine, Shendong Coalfield, China. *Remote Sens.* **2016**, *8*, 951–976. [CrossRef]
18. Xiong, S.; Muller, J.P.; Li, G. The application of ALOS/PALSAR InSAR to measure subsurface penetration depths in deserts. *Remote Sens.* **2017**, *9*, 638. [CrossRef]
19. Natsuaki, R.; Nagai, H.; Motohka, T.; Ohki, M.; Watanabe, M.; Thapa, R.B.; Tadono, T.; Shimada, M.; Suzuki, S. SAR interferometry using ALOS-2 PALSAR-2 data for the Mw 7.8 Gorkha, Nepal earthquake. *Earth Planets Space* **2016**, *68*. [CrossRef]
20. Qu, F.; Zhang, Q.; Lu, Z.; Zhao, C. Yang, C.; Zhang, J. Land subsidence and ground fissures in Xi'an , China 2005–2012 revealed by multi-band InSAR time-series analysis Remote Sensing of Environment Land subsidence and ground fi ssures in Xi'an , China 2005–2012 revealed by multi-band InSAR time-series analysis. *Remote Sens. Environ.* **2014**, *155*, 366–376.
21. Wegmüller, U.; Member, S.; Walter, D.; Spreckels, V.; Werner. C.L.; Member, S. Nonuniform Ground Motion Monitoring with TerraSAR-X Persistent Scatterer Interferometry. *IEEE Trans. Geosci. Remote Sens.* **2010**, *48*, 895–904. [CrossRef]
22. Tarchi, D.; Casagli, N.; Fanti, R.; Leva, D.D.; Luzi, G.; Pasuto, A.; Pieraccini, M.; Silvano, S. Landslide monitoring by using ground-based SAR interferometry: An example of application to the Tessina landslide in Italy. *Eng. Geol.* **2003**, *68*, 15–30. [CrossRef]
23. InSAR Technical Background. Available online: https://skygeo.com/insar-technical-background/ (accessed on 5 July 2021).
24. Venmans, A.A.M.; de Kelder, M.; de Jong, J.; Korff, M.; Houtepen, M. Reliability of InSAR satellite monitoring of buildings nearinner city quay walls. *Proc. IAHS* **2020**, *382*, 195–199. [CrossRef]
25. Van Leijen, F.J. Persistent Scatterer Interferometry Based on Geodetic Estimation Theory. Ph.D. Thesis, Delft University of Technology, Delft, The Netherlends, 2014, doi:10.4233/uuid:5dba48d7-ee26-4449-b674-caa8df93e71e [CrossRef]
26. Lenda, G.; Uznanski, A.; Strach, M. Influence of time delays of robotic total stations with high sampling frequency on accuracy of measurements to moving prisms. *Arch. Civ. Eng.* **2019**, *LXV*, 31–48. [CrossRef]
27. Terzaghi, K. *Theoretical Soil Mechanics*; John Wiley and Sons, Inc.: New York, NY, USA, 1943. [CrossRef]
28. Peck, R.B. Advantages and limitations of the observational method in applied soil mechanics. *Geotechnique* **1969** *19*, 171–187. [CrossRef]
29. Mazzanti, P. Toward Transportation Asset Management: What is the role of geotechnical monitoring? *J. Civ. Struct. Health Monit.* **2017**, *7*, 645–656. [CrossRef]
30. Chung, W.W.S.; Tariq, S.; Mohandes, S.R.; Zayed, T. IoT-based application for construction site safety monitoring. *Int. J. Constr. Manag.* **2020**, 1–17. [CrossRef]
31. Sharkar, D.; Patel, H.; Dave, B. Development of integrated cloud-based Internet of Things (IoT) platform for asset management of elevated metro rail projects. *Int. J. Constr. Manag.* **2020**, 1–10. [CrossRef]
32. Bartoli, A.; Guilhot, D.; Vilajosana, X. Boosting a More Efficient Tailings Dam Risk Management Service through an Innovative IoT Ecosystem. In Proceedings of the 24th International Conference on Tailings Mine Waste, Fort Collins, CO, USA, 15 November 2020; pp. 649–660.
33. Milkulenas, V.; Minkevicius, V.; Satkunas, J. Gediminas's Castle Hill (in Vilnius) case: Slopes failure through historical times until present. *Proc. World Landslide Forum* **2017**, *4*, 69–76.
34. 2020 Was Lithuania's Warmest Year on Record. Available online: https://www.delfi.lt/en/lifestyle/2020-was-lithuanias-warmest-year-on-record.d?id=86157103 (accessed on 8 June 2021).
35. Treuhaft, R.N.; Law, B.E.; Asner, G.P. Forest Attributes from Radar Interferometric Structure and Its Fusion with Optical Remote Sensing. *BioScience* **2004**, *54*, 561–571. [CrossRef]
36. Carlà, T.; Tofani, V.; Lombardi, L.; Raspini, F.; Bianchini, S.; Bertolo, D.; Thuegaz, P.; Casagli, N. Combination of GNSS, satellite InSAR, and GBInSAR remote sensing monitoring to improve the understanding of a large landslide in high alpine environment. *Geomorphology* **2019**, *335*, 62–75. [CrossRef]
37. Wei, M.; Sandwell, D.; Smith-Konter, B. Optimal combination of InSAR and GPS for measuring interseismic crustal deformation. *Adv. Space Res.* **2010**, *46*, 236–249. [CrossRef]
38. Carlà, T.; Farina, P.; Intrieri, E.; Ketizmen, H.; Casagli, N. Integration of ground-based radar and satellite InSAR data for the analysis of an unexpected slope failure in an open-pit mine. *Eng. Geol.* **2018**, *235*, 39–52. [CrossRef]
39. Shamshiri, R.; Motagh, M.; Maes, M.; Sharifi M.A. Insar and Finite Element Analysis of Ground Deformation at Lake Urmia Causeway (luc), Northwest Iran. *Int. Arch. Photogramm. Remote Sens. Spat. Inf. Sci.* **2013**, *w3*, 389–391 [CrossRef]
40. Available online: https://site.tre-altamira.com/rocscience-3d-slope-stability-programs-now-integrated-with-our-satellite-insar-data/ (accessed on 24 August 2020).
41. Selvakumaran, S.; Rossi, C.; Marinoni, A.; Webb, G.; Bennetts, J.; Barton, E.; Plank, S.; Middleton, C. Combined InSAR and Terrestrial Structural Monitoring of Bridges. *IEEE Trans. Geosci. Remote Sens.* **2020** *58*, 7141–7153. [CrossRef]

42. Lastra, A.; Gonzalez, P.; Beniamino, R.; Rodriguez Solá, R.; Ribalaygua, J. Escenarios de cambio climático para eventos pluviométricos severos en la Comunidad de Madrid. In *Cuadernos de I+D+i 27*; Canal de Isabel II: Madrid, Spain, 2018.
43. DiMartire, D.; Iglesias, R.; Monells, D.; Centolanza, G.; Sica, S.; Ramondini, M.; Pagano, L.; Mallorqui, J.; Calcaterra, D. Comparison between Differential SAR interferometry and ground measurements data in the displacement monitoring of the earth-dam of Conza della Campania (Italy). *Remote Sens. Environ.* **2014**, *148*, 58–69. [CrossRef]
44. Tofani, V.; Raspini, F.; Catani, F.; Casagli, N. Persistent Scatterer Interferometry (PSI) Technique for Landslide Characterization and Monitoring. *Remote Sens.* **2013**, *5*, 1045–1065. [CrossRef]
45. Antronico, L.; Borrelli, L.; Peduto, D.; Fornaro, G.; Gulla, G.; Paglia, L.; Zeni, G. Conventional and Innovative Techniquesfor the Monitoring of Displacementsin Landslide Affected Area. In *Landslide Science and Practice*; Margottini, C., Canuti, P., Sassa K., Eds; Springer: Berlin/Heidelberg, Germany, 2013; pp. 125–131.
46. Salem, M.; El-Sherbiny, R. Comparison of measured and calculated consolidation settlements of thick underconsolidated clay. *Alex. Eng. J.* **2013**. [CrossRef]
47. Wasswa, B.; Kakitahi, D.; JJuuko, S.; Semuwemba, J.; Kalumba, D. Study of Slope Stability and Settlement Characteristics of Mpererwe Landfill. In Proceedings of the Pan American Conference on Soil Mechanics and Geotechnical Engineering, Buenos Aires, Argentina, 15–18 November 2015.